Hindawi
International Journal of Photoenergy
Volume 2019, Article ID 7432848, 17 pages
https://doi.org/10.1155/2019/7432848

Research Article

Photosynthetic Pigments with Potential for a Photosynthetic Antenna: A DFT Analysis

Jesús Francisco Monzón-Bensojo,[1] Manuel A. Flores-Hidalgo,[2] and Diana Barraza-Jiménez[2]

[1]*Centro de Investigación en Alimentación y Desarrollo, A.C. Unidad Delicias, Av. 4ª Sur 3820, Fracc. Vencedores del Desierto. 33089, Cd. Delicias, CHIH, Mexico*
[2]*Universidad Juárez del Estado de Durango, Facultad de Ciencias Químicas, Ave. Veterinaria s/n, Circuito Universitario, 34120 Durango, Mexico*

Correspondence should be addressed to Diana Barraza-Jiménez; dianabarraza@ujed.mx

Received 14 September 2018; Revised 19 December 2018; Accepted 17 January 2019; Published 2 April 2019

Guest Editor: Chunling Wang

Geometrical and electronic properties of the main photosynthetic pigments in higher plants such as chlorophylls and xanthophylls were studied to find potential candidates that were able to participate in an eventual zeolite-dye artificial antenna. CRDFT (chemical reactivity density functional theory) and TD-DFT (time-dependent DFT) methods were employed in ground-state and excited-state calculations, respectively. The evaluated electronic properties at the gas phase included (a) energies such as HOMO-LUMO band gap (*H-L*, ranging from 2.168 to 2.504 eV), adiabatic ionization potential (*I*, ranging from 5.964 to 7.207 eV), and adiabatic electronic affinity (*A*, ranging from 2.176 to 2.741 eV); (b) global chemical reactivity indexes such as electronegativity (χ, ranging from 4.121 to 4.974 eV), hardness (η, ranging from 1.812 to 2.233 eV), electrophilicity index (ω, ranging from 4.365 to 5.541 eV), and electroaccepting-electrodonating powers (ω^+, ranging from 1.671 to 2.115 eV, and ω^-, ranging from 4.375 to 5.273 eV); (c) electron-hole reorganization energies (λ, ranging from 0.225 to 0.519 eV and ranging from 0.168 to 0.425 eV, respectively) and electron-hole extraction potentials (*EEP*, ranging from 2.570 to 2.966 eV, and *HEP*, ranging from 5.538 to 7.012 eV, respectively); and (d) local chemical reactivity indexes like condensed Fukui functions (f_k), condensed dual descriptor ($f^{(2)}(r)$), and condensed local softness (s_k). These electronic properties allowed the association between molecules and reactivity-selectivity criteria, under the context of charge transfer and electronic transitions. Also, the aforementioned electronic properties were determined for combinations made with the selected molecules (β-cryptoxanthin and zeaxanthin) and 5 solvents (*n*-hexane, diethyl ether, acetone, ethanol, and methanol) with upward dielectric constants (ε). From frequency calculations, IR spectra were obtained for combinations. Finally, excited-state computations were carried out to acquire UV-Vis spectra of the combinations. We conclude that the selection of dyes is controlled mainly by geometrical constraints rather than by electronic properties.

1. Introduction

Mankind dependence on fossil fuels has drastically increased greenhouse gases in the earth's atmosphere. Gases are responsible for global warming, a major threat faced by humanity. Ecosystem destruction, biodiversity loss, disease proliferation, drought, and glacier melting are effects of this threat. For mitigation of global warming, development of alternative energy sources must be implemented [1].

These sources can avoid our dependence on fossil fuels to deal with such a challenging threat. They should be abundant, economic, ecofriendly, and ubiquitous. Sunlight complies with these requirements, and it is abundant; sun emissions toward the earth are ~120 PW. Harvesting sunlight during the day would allow mankind to satisfy its energy needs for more than 27 years [2].

Photosynthesis takes advantage of sunlight and may be split into 2 steps: the first step is denominated light reactions,

and the second one is termed carbon fixation reactions. During light reactions, light-harvesting complexes (LHCs) carry out energy harvesting and transferring, and energy is directed toward 2 reaction centers (photosystem I and photosystem II), where chlorophyll *a* starts an electron transport chain. In photosystem II, water is transformed into oxygen and protons, and electrons gotten from chlorophyll *a* and protons are employed to synthesize $NADPH_2$ and ATP, respectively. Both compounds are utilized in the next step where atmospheric carbon dioxide is fixed to synthetize carbohydrates [3]. Photosynthetic pigments (chlorophylls and carotenoids) present in LHCs lodge in protein matrices where they harvest and transfer energy with efficiencies fluctuating between 95% and 99% [3].

Chlorophylls and carotenoids possess a chromophore; the former have a porphyrin coplanar conjugated ring while the latter have a central coplanar conjugated hydrocarbonated chain. Both chromophores have a delocalized π electron system that is responsible for electronic transitions and electron transfer. Carotenoids usually exhibit an intense absorption band, typically in the 400–500 nm range. This electronic transition is from the ground state (S_0) to the second excited singlet state (S_2), instead of heading to the first excited singlet state (S_1), since the transition from S_0 to S_1 is forbidden because of the symmetry of the carotenoid molecule. With both the S_2 and S_1 states having exceptionally short lifetimes, it is perhaps surprising that carotenoids are able to carry out energy transfer to chlorophylls before they decay releasing heat. Yet, in many cases, carotenoids are efficient antenna pigments, because the energy transfer process is even faster than the deactivation rate [4, 5].

In higher plants, the dyes involved in harvesting and transferring energy are chlorophylls *a* and *b* as well as xanthophylls: β-cryptoxanthin, lutein, zeaxanthin, violaxanthin, and neoxanthin. Xanthophylls' aforesaid most abundant isomers are usually *trans* (being 9-*cis*-violaxanthin an exception) [6]. Another important isomer is 9′-*cis*-neoxanthin whose location in spinach's photosystem II LHCs has been elucidated by X-ray techniques; they have demonstrated that this isomer may transfer energy exclusively to chlorophyll *b* [7], and experimental evidence supports this assertion [8, 9].

Artificial photosynthesis inspires itself in natural photosynthesis; the objective of the former is designing systems to convert sunlight into other useful kinds of energy (e.g., electricity), intending to mitigate the global warming threat. Systems include (1) molecules that harvest and transfer sunlight into a reaction center; (2) a reaction center; (3) a complex that transforms water into electrons, protons, and oxygen; and (4) a reducing agent to produce fuels [10].

Luminescent solar concentrators (LSCs) possess host systems that harbor molecules inside zeolite. Lynde Type "L" is a robust zeolite system; it is a microporous material with an empirical formula $(M^+)_9[(AlO_2)_9(SiO_2)_{27}]_9{\cdot}(16\text{-}21)H_2O$. Zeolite crystals contain many nanometric channels aligned following a parallel ordering among them. These nanochannels are unidimensional, and their pore diameter is 7.1 Å. A channel is a succession of unit cells, and the unit cell length is 7.5 Å. In the inner channels, synthetic molecules can harvest and transfer energy to a reaction center via the FRET (Förster resonance energy transfer) mechanism. Zeolite morphology enables the inclusion of a great number of molecules. For example, a 30×30 nm crystal contains ~240 nanochannels that may host ~4800 molecules if each molecule occupies 2-unit cells. Besides, molecular confinement orientates electronic transition dipole moments (ETDM) parallel to the channel, which is a feature that increases FRET efficiency [11].

Before evaluating the theoretical FRET efficiency of an artificial antenna (during subsequent computations not presented in this work), there must be a selection of the pigments that will be employed later, which is one of the aims of the present work. Previously, chemical reactivity indexes derived from conceptual CRDFT have been used, as well as energies (*H-L*, *I*, and *A*), to correlate them with the theoretical efficiency of a dye-sensitized solar cell which uses these kinds of dyes [12] and to assess theoretically carotenoids as potential candidates for a solar energy-harvesting device [13]. The general objective of the current research is to find photosynthetic pigments capable of participating in a zeolite-dye system. Employing natural molecules offers advantages as they are abundant, cheap, ecofriendly, and ubiquitous.

2. Computational Details

Calculations were done in the Gaussian 09 software suite [14] using DFT [15] in ground-state computations and TD-DFT [16] for excited states. DFT is a robust level of theory to study molecules in their ground state, while TD-DFT is a widely used methodology to compute excited states, including those related to carotenoids and sensitizers for solar cells [13, 17].

Methyl chlorophyllides did not include their phytyl tail during calculations because this tail is employed exclusively to anchor the molecule to its hydrophobic environment and does not participate either in electronic transitions or in electron transfer [18].

Initial molecular structures were downloaded from the ChemSpider website (http://www.chemspider.com/) and were drawn with ChemDraw Ultra v.12.0 software [19]. The trivial name, abbreviation, and ChemSpider ID of the assessed dyes were methyl chlorophyllide *a*/CHLA/388735, methyl chlorophyllide *b*/CHLB/34999392, all-*trans*-β-cryptoxanthin/BCRY/4444647, all-*trans*-zeaxanthin/ZEA/4444421, all-*trans*-lutein/LUT/4444655, 9-*cis*-violaxanthin/VIO/4445401, all-*trans*-neoxanthin/NEO/4444659, and 9′-*cis*-neoxanthin/9NEO/4445400.

Regardless of the good performance of B3LYP hybrid functional in assessing a variety of properties such as molecular adsorption in cluster models of zeolite [20] or geometry and electronic properties of carotenoids [13], other hybrid functionals such as B3P86 should be tested. This functional has been less reported in literature, particularly in evaluating geometry and electronic properties of photosynthetic pigments. Comparing its performance with respect to B3LYP might contribute to the theoretical study of photosynthetic dyes.

Methodology may be split into 2 steps. In the first step, calculations carried out during pigment screening were in

the gas phase; the B3P86 hybrid functional (Becke contributes with 3 parameters of electron exchange and Perdew contributes with a nonlocal correlation functional created in 1986) [21, 22] was utilized in geometry, frequency, and energy computations. The 6-31G(d) Pople basis set [23] was employed as the starting point for geometry and frequency calculations; ground-state energies were calculated using a more robust 6-31+G(d,p) basis set. From energies, *H-L*, adiabatic *I*, and adiabatic *A* were obtained, and with these values, global and local chemical reactivity indexes were evaluated [24]. The molar volume was computed by adding the keyword "volume" to the geometry optimization. Each pigment received a punctuation based on the contribution of their properties to electronic transitions and electron transfer. Statistical tests were conducted to assess dye and property scores, data normality and variance equality were evaluated, and subsequently, one-way Kruskal-Wallis and ANOVA tests were carried out to detect differences ($p < 0.05$) among dye and property scores, respectively. Fisher's LSD multiple-comparison test was performed to find which property's means were different among them; NCSS 2006 software was used to carry out the statistical tests [25].

In the second step, the selected molecules (BCRY and ZEA) were combined with different solvents (Hex = *n*-hexane ($\varepsilon = 1.8819$), Et_2O = diethyl ether ($\varepsilon = 4.2400$), Ace = acetone ($\varepsilon = 20.9430$), EtOH = ethanol ($\varepsilon = 24.8520$), and MeOH = methanol ($\varepsilon = 32.6130$)). The combinations were evaluated with CAM-B3LYP hybrid functional [26] and with an even more robust 6-311+G(d,p) basis set [27] to perform geometry, frequency, and energy computations in ground and excited states. CAM-B3LYP is a long-range-corrected functional; it has been used to assess electronic coupling between $1^1B_u^+$ carotenoid electronic states and chlorophyll Soret band states in photosystem II's LHCs of higher plants [28]. Also, it has succeeded in studying the electronic excitations in VIO and ZEA [29], and geometry and electronic property calculations with this functional have not been performed yet for the full set of photosynthetic dyes within higher plants. IR spectra were derived from frequency results while λ, *EEP*, and *HEP* were obtained from adiabatic energies during step 1 and step 2. PCM (polarizable continuum solvation model) was employed in the present work because of its 2 main characteristics, namely, the use of a molecular cavity following the real geometry of the investigated system and the use of a surface charge distribution to represent the polarization of the environment [30]. Finally, 10 excited states were computed using the Tamm-Dancoff approximation, and UV-Vis spectra were obtained from the electronic transition from S_0 to S_2.

3. Results and Discussion

3.1. Molecular Geometry. All molecular structures are displayed in Figures 1(a) and 1(b) while the molecular size of photosynthetic pigments is shown in Table 1. Regardless of the quantum nature of matter, when the inclusion of a molecule within a host system is simulated computationally, it is essential to know if the molecular size will allow the molecule to fit into the host system's cavities.

After the geometry optimization of our molecules, the maximum molecular length along the *x*, *y*, and *z* Cartesian axes was measured (Supplementary Materials, Tables 1–8). The molecular size of our set of dyes had not been reported before in the literature. Beginning with this information, other theoretical researchers will be able to choose among our molecules and the available host systems, to carry out simulations different from those reported in this work. Molecular size contributes to the geometry characterization of a molecule, similarly to bond distances, bond angles, and dihedral angles. In fact, molecular size is the synthesis of these last three parameters.

Recently, we performed a calculation, where the geometry of ZEA was optimized inside the zeolite in the gas phase (since the present work deals exclusively with computations carried out outside the zeolite, calculations performed inside the zeolite are going to be presented in a subsequent article). The result was the strong electric fields of the zeolite distorting the molecular geometry, but thanks to the measurement of the molecular size, we knew that *y* maximum length decreased from 6.4 to 5.4 Å, *z* maximum length increased from 5.8 to 6.0 Å, and *x* maximum length increased from 31.4 to 31.8 Å, once compared with their counterparts (outside the zeolite in the gas phase). Certainly, zeolite confinement will never allow molecules to undergo a distortion beyond the zeolite pore diameter (7.1 Å).

The *y* maximum and *z* maximum lengths decide ultimately if the pigment will fit into the zeolite cavity. In this regard, it is obvious from Table 1 that only BCRY and ZEA fulfill this requisite (<7.1 Å). In the case of *x* maximum length, there are 2 issues that must be pointed out. Firstly, dye length allows the molecule to remain parallel to the nanochannel without the inconvenience of the molecule's free rotation because of short length (<7.1 Å). Secondly, the more parallel the orientation of the pigment along the *x* -axis, the higher the FRET efficiency, because the ETDM is also parallel to the *x*-axis [11]. In the case of methyl chlorophyllides, their *x* maximum lengths are ~12 Å, so these pigments would occupy about 1.6 zeolite's unit cells; meanwhile, xanthophylls with ~30 Å would fill about 4 zeolite's unit cells.

Additional observations from Table 1 may be that BCRY-B3P86-GP (gas phase) has a smaller *y* maximum length than BCRY/CAM-B3LYP/GP with a difference of 0.3 Å between them. Something similar happens with ZEA-B3P86-GP where *y* and *z* maximum lengths are smaller than those of ZEA/CAM-B3LYP/GP by 0.2 and 0.3 Å, respectively. In the case of ZEA combinations, one can observe how ZEA-Ace and ZEA-MeOH with identical *x*, *y*, and *z* maximum lengths have very similar molar volumes (796.9 and 796.5 $Å^3$, respectively). Consistently, ZEA-EtOH has the smallest *z* maximum length among ZEA combinations (5.8 Å) and also the lowest molar volume (707.6 $Å^3$). Molar volume is just a supplementary datum which does not determine if a molecule fits into a zeolite nanochannel as molecular size does.

3.2. Molecular Properties. Before discussing this section, it is convenient to take into account molecular property suitability (MPS), which was based on their contribution to electronic

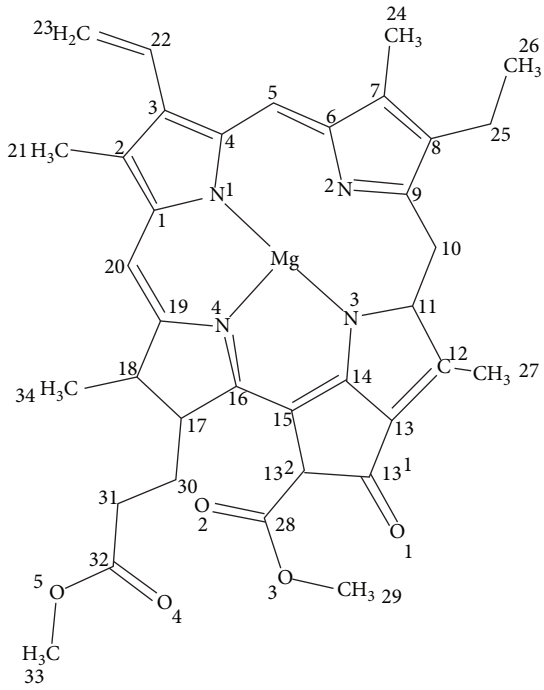

(A)

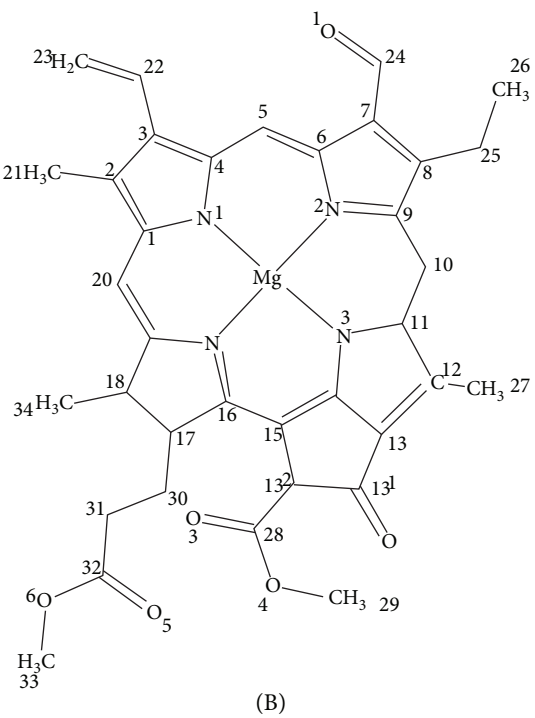

(B)

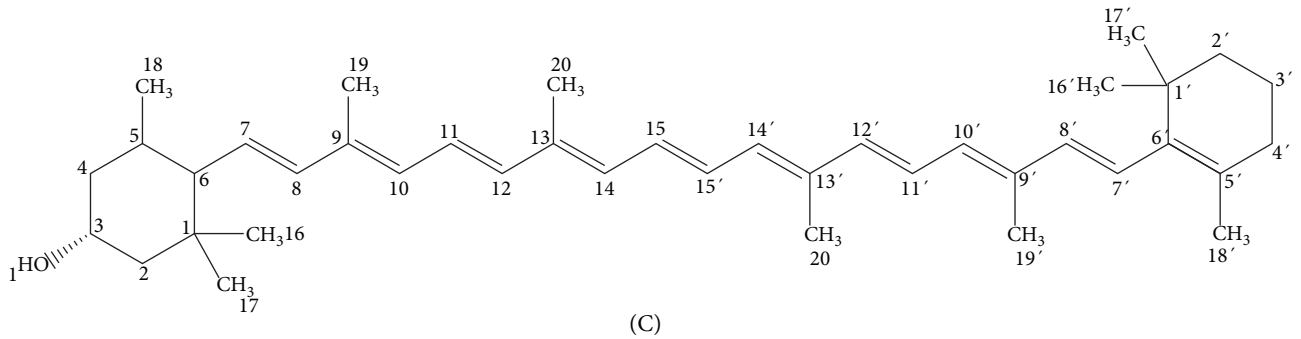

(C)

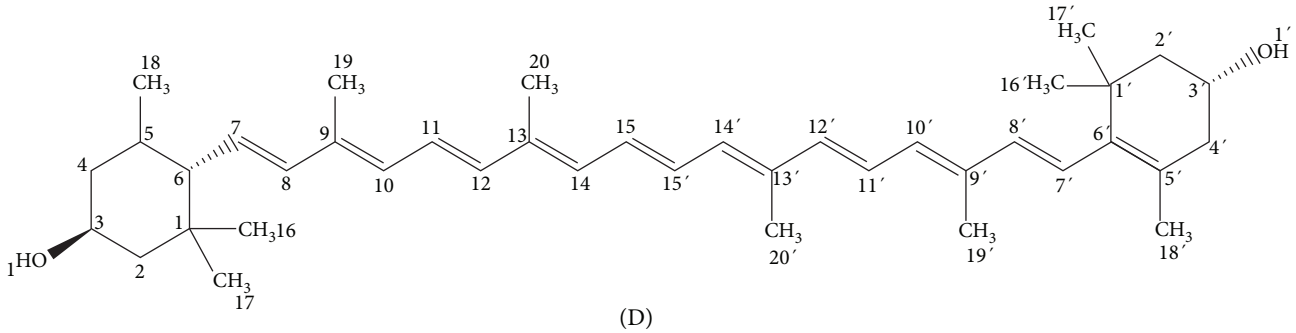

(D)

(a)

Figure 1: Continued.

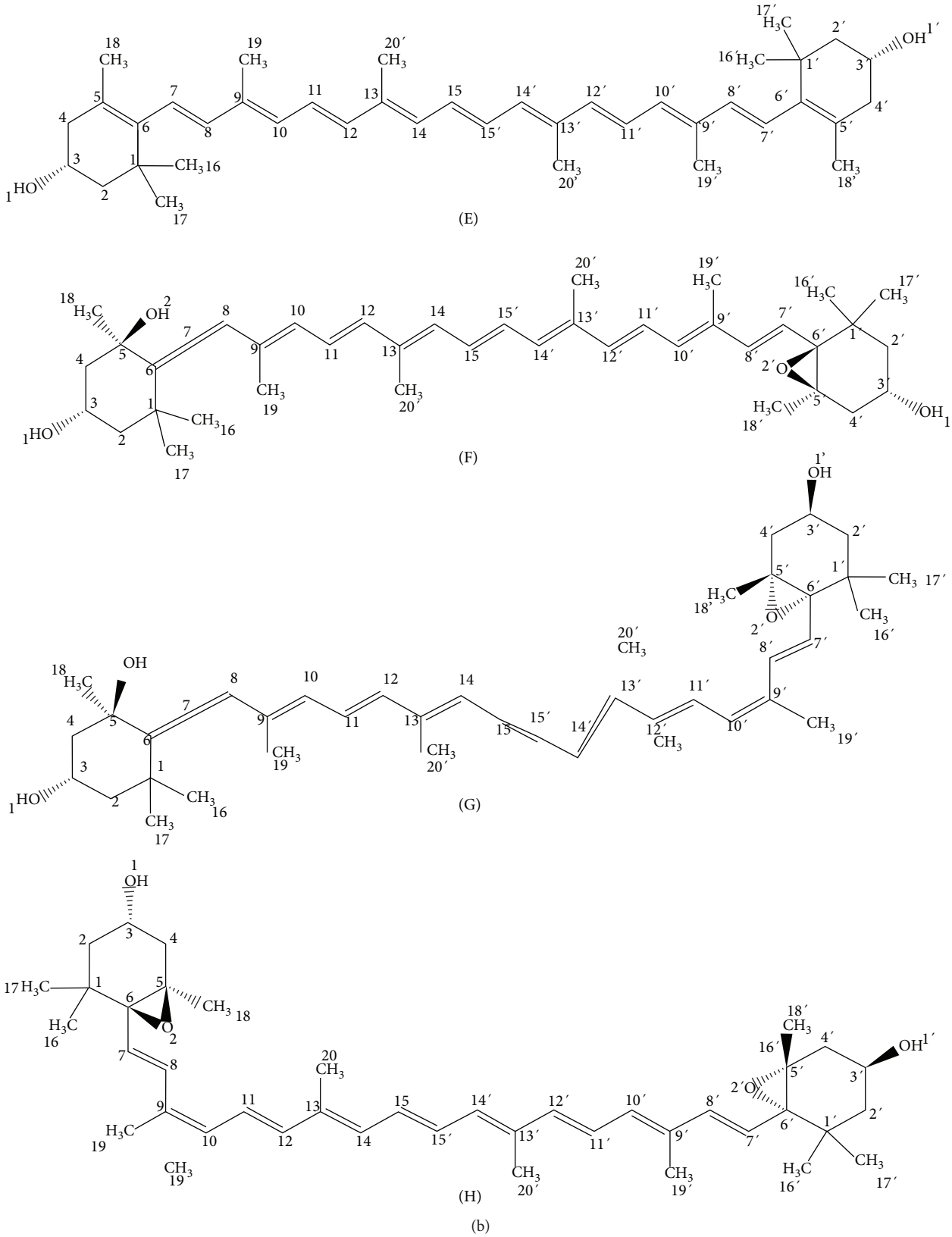

Figure 1: (a) Structures for (A) methyl chlorophyllide *a*, (B) methyl chlorophyllide *b*, (C) all-*trans*-β-cryptoxanthin, and (D) all-*trans*-lutein. (b) Structures for (E) all-*trans*-zeaxanthin, (F) all-*trans*-neoxanthin, (G) 9′-*cis*-neoxanthin, and (H) 9-*cis*-violaxanthin.

Table 1: Molecular size of pigments under study.

Molecule or combination	x maximum length (Å)	y maximum length (Å)	z maximum length (Å)	Molar volume (Å^3)
CHLA	12.2	15.3	8.6	780.9
CHLB	12.3	15.5	8.7	660.1
BCRY[1]	30.8	6.1	5.0	786.7
BCRY[2]	30.7	6.1	5.3	898.1
ZEA[1]	31.3	6.4	5.8	750.8
ZEA[2]	31.3	6.6	6.1	848.3
LUT	29.9	7.3	6.1	964.2
VIO	27.4	9.6	6.4	870.5
NEO	28.4	7.2	6.7	734.6
9NEO	24.3	10.2	6.7	847.1
BCRY-Hex	30.7	6.1	5.2	866.8
BCRY-Et_2O	30.7	6.1	5.2	798.8
BCRY-Ace	30.7	6.1	5.2	907.9
BCRY-EtOH	30.7	6.1	5.2	783.2
BCRY-MeOH	30.7	6.1	5.2	827.0
ZEA-Hex	31.3	6.6	6.0	877.5
ZEA-Et_2O	31.3	6.6	6.0	805.9
ZEA-Ace	31.3	6.5	6.0	796.9
ZEA-EtOH	31.4	6.6	5.8	707.6
ZEA-MeOH	31.3	6.5	6.0	796.5

The utilized functionals were [1]B3P86 and [2]CAM-B3LYP.

transitions and electron transfer. Equations to calculate these properties are available in Supplementary Materials.

Table 2 displays energy values and chemical reactivity indexes for the tested pigments. Starting with *H-L*, it is defined as the energy needed to enable an electron from the *HOMO* (S_0 for carotenoids) to undertake an electronic transition to the *LUMO* (S_2 for carotenoids) [4, 31]. Given that visible sunlight ranging from 400 to 700 nm constitutes ca. 39% of spectral solar irradiance [32], *H-L* of a light-harvesting molecule should fall within ~1.7-3.1 eV. Within the latter range, the value of this property should be as low as possible, because either a 400 nm photon or a 700 nm photon would promote the necessary electronic transition to start FRET, from a donor molecule to an acceptor molecule. It should be noted that *H-L* gaps predicted by the majority of density functional approximations are underestimated due to the self-interaction error and not containing the information provided by the discontinuities with respect to the number of electrons of the derivatives of the exchange-correlation energy. The molecule with the lowest *H-L* is BCRY (2.168 eV) which works at 572 nm whereas the pigment with the highest *H-L* is CHLB (2.504 eV) which works at 495 nm. Then, MPS followed the next order: BCRY > ZEA > LUT > NEO > VIO > 9NEO > CHLA > CHLB. Experimental *H-L* for ZEA in Hex is 2.60 eV [33], which is underestimated by 0.43 eV by our study. The *H-L* provided by generalized gradient approximations (GGAs) and hybrid functionals is smaller than the experimental one, a good *H-L* average for carotenoids is about 2.400 eV [34], and all theoretical carotenoids' *H-L*s are below the latter value. Regarding chlorophylls' *H-L*s, it should be reminded that due to configuration interactions among the 4 Gouterman π molecular orbitals, it is not correct to state that electronic transitions reflect a simple promotion of an electron from HOMO to LUMO. For instance, experimental excitation energies of Q_y, Q_x, and B bands for CHLA are 1.88, 2.16, and 2.90 eV, respectively [35]. Our results estimated that *H-L* (2.374) is found between Q_x and B bands.

By definition, I is the needed energy to extract an electron from a neutral molecule in order to form a cation. A high value of this property is closely related to the stiffness of the electronic cloud. In terms of reactivity, the cloud is more reluctant to participate in electron transfer. Consequently, the lower the ionization potential value, the higher the molecular potential to serve as an electron donor. The molecule with the lower I was NEO (5.964 eV), and the highest value was held by CHLB (7.207 eV). MPS is ordered in the following way: NEO > BCRY > ZEA > 9NEO > LUT > VIO > CHLA > CHLB.

With respect to A, it is well known that it deals with the energy released when a neutral molecule accepts an electron to form an anion. Soft electronic clouds are more prone to accept an electron, becoming into an attractive choice for being suitable acceptors. The higher the electronic affinity value, the higher the molecular potential for representing a good charge acceptor. The molecule with the highest A was CHLB (2.741 eV), and the molecule with the lowest value was 9NEO (2.176 eV). MPS is ordered in the following way: CHLB > CHLA > ZEA > LUT > BCRY > NEO > VIO > 9NEO.

Regarding χ, it is defined as the capacity of a molecule to attract electrons [36]. This property is closely related to electronic affinity and ionization potential. As it happens with electronic affinity, the higher the value, the higher its suitability to act as a charge acceptor. The molecule with the highest value is CHLB (4.974 eV), and the lowest value is held by 9NEO (4.121 eV). MPS is ordered in the following way: CHLB > CHLA > VIO > LUT > ZEA > BCRY > NEO > 9NEO.

η is interpreted as the resistance of an electronic cloud to involve itself in electron transfer [37]. The lower its value, the better its performance both to accept and to transfer charge successfully. The pigment with the lowest value was NEO (1.812 eV), and the dye with the highest value was CHLB (2.233 eV). MPS is ordered in the following way: NEO > BCRY-ZEA > 9NEO > LUT > VIO > CHLA > CHLB.

In connection with ω, it measures the ability of a molecule for getting saturated with electrons in maximum flux conditions [38]. Despite the fact that some authors have previously suggested that its value should be as low as possible, in order to improve the performance of theoretically assessed solar cells and artificial devices [12, 13], our work and results suggest that desirable values for this property must be as high as possible, since it is conceived by its originators like a kind of power, and appropriate power values are usually needed to be as high as possible. Besides, in preliminary calculations ω of one of the most used synthetic dyes inside zeolite

Table 2: Associated energies and chemical reactivity indexes (EP (electronic properties)) for the tested pigments at the gas phase (highest values are shown for local reactivity indexes).

Electronic property	CHLB	CHLA	LUT	NEO	ZEA	BCRY	VIO	9NEO
H-L (eV)	2.504	2.374	2.216	2.237	2.170	2.168	2.296	2.306
I (eV)	7.207	6.880	6.108	5.964	6.036	5.994	6.210	6.066
A (eV)	2.741	2.519	2.347	2.340	2.366	2.323	2.299	2.176
χ (eV)	4.974	4.700	4.228	4.152	4.201	4.159	4.255	4.121
μ (eV)	-4.974	-4.700	-4.228	-4.152	-4.201	-4.159	-4.255	-4.121
η (eV)	2.233	2.181	1.880	1.812	1.835	1.835	1.956	1.945
S (eV)	0.448	0.459	0.532	0.552	0.545	0.545	0.511	0.514
ω (eV)	5.541	5.064	4.753	4.757	4.809	4.712	4.627	4.365
ω^- (eV)	5.273	4.986	4.480	4.397	4.450	4.406	4.513	4.375
$\omega+$ (eV)	2.115	1.938	1.813	1.811	1.831	1.796	1.770	1.671
$\Delta\omega^{\pm}$ (eV)	7.388	6.924	6.293	6.208	6.281	6.202	6.283	6.046
f_k^+	0.069	0.073	0.055	0.054	0.053	0.053	0.057	0.056
Atom	C(23)	C(23)	C(11)	C(7′)	C(11′)	C(11′)	C(11′)	C(7)
f_k^-	0.059	0.062	0.054	0.054	0.050	0.050	0.056	0.055
Atom	C(23)	C(23)	C(7)	C(7′)	C(7′)	C(7′)	C(7′)	C(16)
f_k^0	0.064	0.067	0.054	0.054	0.050	0.050	0.055	0.055
Atom	C(23)	C(23)	C(7)	C(7′)	C(7′)	C(7)	C(11′)	C(7)
$f^{(2)}(r)^+$	0.042	0.037	0.008	0.007	0.007	0.009	0.006	0.007
Atom	C(10)	C(10)	C(15′)	C(12′)	C(15′)	C(15′)	C(15)	C(7′)
$f^{(2)}(r)^-$	-0.034	-0.032	-0.014	-0.005	-0.006	-0.007	-0.004	-0.006
Atom	C(9)	C(9)	C(13′)	C(14)	C(10′)	C(10′)	C(10′)	C(6)
s_k^+ (eV)	0.031	0.033	0.029	0.030	0.029	0.029	0.029	0.029
Atom	C(23)	C(23)	C(11)	C(7′)	C(11′)	C(11′)	C(11′)	C(7)
s_k^- (eV)	0.027	0.028	0.029	0.030	0.027	0.027	0.029	0.028
Atom	C(23)	C(23)	C(7)	C(7′)	C(7′)	C(7′)	C(7′)	C(16)
s_k^0 (eV)	0.029	0.031	0.029	0.030	0.027	0.027	0.028	0.028
Atom	C(23)	C(23)	C(7)	C(7′)	C(7′)	C(7)	C(11′)	C(7)
λ_e (eV)	0.225	0.226	0.337	0.519	0.335	0.327	0.349	0.395
EEP (eV)	2.966	2.745	2.684	2.859	2.701	2.650	2.648	2.570
λ_h (eV)	0.195	0.168	0.325	0.425	0.332	0.333	0.295	0.324
HEP (eV)	7.012	6.712	5.783	5.538	5.705	5.661	5.915	5.742

(pyronine molecule) [11] and found a very high value of 12.139 eV. CHLB had the maximum value (5.541 eV) while 9NEO (4.365 eV) presented the lowest one. MPS is ordered in the following way: CHLB > CHLA > ZEA > NEO > LUT > BCRY > VIO > 9NEO.

Focusing on ω^- and ω^+, they are related to the molecular ability of donating and accepting charge, respectively. The former is desirable to be as low as possible, whereas the latter is recommendable to be as high as possible [39]. 9NEO has the lowest ω^- (4.375 eV) while CHLB (5.273 eV) has the highest one. MPS is ordered in the following way: 9NEO > NEO > BCRY > ZEA > LUT > VIO > CHLA > CHLB. On the other hand, CHLB had the highest ω^+ (2.115 eV) while 9NEO has the lowest one (1.671). MPS is ordered in the following way: CHLB > CHLA > ZEA > LUT > NEO > BCRY > VIO > 9NEO. From values of both indexes, it can be inferred that pigments under study are better donors than acceptors. MPS of ω and ω^+ is almost identical because both properties measure the molecule's ability to act as a good acceptor. In the case of ω^-, it does not present just the converse order of its counterpart, since VIO and NEO are exceptions, showing the need of calculating this property.

Regarding local chemical reactivity indexes, f_k and $f^{(2)}(r)$ showed no correlation between them at the time of detecting the atoms more prone to nucleophilic and electrophilic attacks. Regardless of the fact that both indexes were different, one would expect some agreement when they are compared. Parameter s_k showed little difference among the sets of evaluated molecules, even between chlorophylls and xanthophylls, to make clear that this local index should not decide which pigments would have better electronic properties. The difference between the highest value and

the lowest value for an atom prone to nucleophilic, electrophilic, and radical attack was barely 0.004, 0.002, and 0.004 eV, respectively.

Finally, λ should be as low as possible in order to avoid wasting solar energy instead of taking advantage of it during the energy transferring process. CHLB had the lowest λ_e (0.225 eV) while NEO had the highest one (0.519). MPS is ordered in the following way: CHLB > CHLA > BCRY > ZEA > LUT > VIO > 9NEO > NEO. CHLA had the lowest λ_h (0.168 eV) while NEO (0.425 eV) had the highest one. MPS is ordered in the following way: CHLA > CHLB > VIO > 9NEO > LUT > ZEA > BCRY > NEO.

Values of Table 2 were used to assign points to each pigment based on MPS, in order to find out which punctuation was received in each case. Equation (1) was employed when the most suitable value of the property is the lowest to optimize electronic transition and/or electron transfer processes.

$$P = \left(1 - \left(\frac{A - B}{B}\right)\right) * 100, \quad (1)$$

where "P" stands for the points obtained by the evaluated molecule, "A" means the property's value assigned for a given molecule, and "B" is the lowest value among tested molecules.

Equation (2) was employed when the most suitable value of the property is the highest to optimize electronic transition and/or electron transfer processes.

$$P = \left(\frac{A}{B}\right) * 100, \quad (2)$$

where "P" denotes the points obtained by the evaluated molecule, "A" stands for the property's value assigned for a given molecule, and "B" is the highest value among tested molecules. An exception is coplanarity (CP) where "B" is not the highest value among tested molecules, but the ideal value (180°). The final scores are displayed in Table 3.

We consider that this punctuation scheme may constitute the basis which motivates other researchers to extend our work by means of more sophisticated mathematical models (such as quantitative structure activity relationships). It must be highlighted that our study has built a 184-data-information matrix (23 properties multiplied by 8 dyes) that will remain available as an initial database. Furthermore, as it will be demonstrated by this research paper following the upcoming discussion, the dyes which will be included in zeolite in future simulations will be chosen due to geometrical constraints instead of their electronic properties.

Talking about comparison among dyes, data were not normal, but they fulfilled variance-equality requirement, so the Kruskal-Wallis test was performed. This test threw a probability level of 0.536, and consequently, there was no difference among dye scores. From a biochemical standpoint, chlorophylls *a* and *b* have an identical ring chemical composition. That is, an *a priori* conclusion of our findings should not be drawn before a set of theoretical calculations. In the case of xanthophylls, the previous argument is also valid with the consideration that xanthophyll central chains are not necessarily identical with respect to their chemical composition. As a partial and careful conclusion, our results suggest that any dye would have the same performance inside zeolite based on their computed properties. Our highest coefficient of variation was held by CHLB (9.7%) which is low enough (say <15.0%) to state that data dispersion of each dye behaved essentially in a homogeneous fashion.

On the other side, since normality and variance-equality assumptions of properties were accomplished, a one-way ANOVA was carried out in order to find the contribution of each property to the score. The probability level was 0.023, and differences among properties were found; these differences were assessed with Fisher's LSD multiple-comparison test. Again, the coefficients of variation exhibited an acceptable dispersion, with hardness becoming the molecule with the highest value (9.7%). Then, *EEP*, η, and s_k^+ did not show a difference with respect to the rest of the properties, so their weight is similar to their counterparts. In a second category, we had the following properties: $\chi, A, \omega, \omega^+$, and *HEP*. The contribution of these properties to the pigment score was considered less relevant than those we will introduce next. Properties which made the main contribution to score include *H-L*, ω^-, *I*, CP, s_k^-, and s_k^0. Surprisingly, the last 2 properties had a significant contribution to score despite the scarce difference between their highest and lowest values. The first 4 properties were the ones which made the greater contribution to score, and their weight was the same. In connection with *H-L*, as it was stated in an aforementioned discussion, it is crucial that the dye harvests both low-energy photons and high-energy photons in order to also maximize its energy transfer ability. ω^- in comparison with ω^+ showed a better capacity to complement the ω values, indicating the importance of a good donor molecule in energy transfer. As we previously say, low *I* attributes pigment a softer electronic cloud more prone to participate in energy transfer processes. Finally, it is well known that at least 1 coplanar structure must be present in a molecule, to take advantage of its delocalized π electron system, in order to carry out energy transfer in a successful way.

The weight of properties (independent variables) was made giving the same weight to each property, and this method is not by far the most adequate one. Nevertheless, we expect to calculate FRET efficiency (the dependent variable) in our subsequent work to correlate it with properties, at least for the 2 selected molecules in the selected solvent. Finally, regardless of the electronic properties and due to geometry constraints, from now on, BCRY and ZEA will be the dyes which will be tested to find the most suitable solvent.

Table 4 shows how the selected properties behave when the dielectric constant ε increases from Hex to MeOH. It is noteworthy that properties change more rapidly from Hex to Ace and then more slightly from Ace to MeOH. For example, BCRY *I* decreased 5.83% from Hex to Et_2O, 3.80% from Et_2O to Ace, 0.17% from Ace to EtOH, and 0.21% from EtOH to MeOH. This behavior showed that MeOH would be the solvent with the highest potential to enhance properties. Also, Ace might be considered like a second option because the increase in property suitability started slowing down slightly once polarity increased from Ace to MeOH.

Table 3: Points obtained by each molecule according to the suitability of its electronic properties (EP).

EP	CHLB	CHLA	LUT	NEO	ZEA	BCRY	VIO	9NEO	$\bar{x}$	S[3]	CV[4]
H-L[1]	84.5	90.5	97.8	96.8	99.9	100.0	94.1	93.6	94.7[a]	5.2	5.5%
ω^{-1}	79.5	86.0	97.6	99.5	98.3	99.3	96.8	100.0	94.6[a]	7.6	8.0%
I[1]	79.2	84.6	97.6	100.0	98.8	99.5	95.9	98.3	94.2[a]	7.9	8.3%
CP	98.7	98.7	99.8	77.5	99.7	99.8	94.0	83.3	93.9[a]	8.7	9.3%
s_k^{-2}	90.0	93.3	96.7	100.0	90.0	90.0	96.7	93.3	93.8[ab]	3.8	4.0%
s_k^{02}	93.5	100.0	93.5	96.8	87.1	87.1	90.3	90.3	92.3[abc]	4.5	4.9%
EEP[2]	100.0	92.5	90.5	96.4	91.1	89.3	89.3	86.6	92.0	4.3	4.7%
η[1]	76.8	79.6	96.2	100.0	98.7	98.7	92.1	92.7	91.9	8.9	9.7%
s_k^{+2}	93.9	100.0	87.9	90.9	87.9	87.9	87.9	87.9	90.5	4.4	4.9%
χ^2	100.0	94.5	85.0	83.5	84.5	83.6	85.5	82.9	87.4[d]	6.3	7.2%
A^2	100.0	91.9	85.6	85.4	86.3	84.8	83.9	79.4	87.2[de]	6.2	7.1%
ω^2	100.0	91.4	85.8	85.9	86.8	85.0	83.5	78.8	87.1[def]	6.3	7.2%
ω^{+2}	100.0	91.6	85.7	85.6	86.6	84.9	83.7	79.0	87.1[defg]	6.2	7.2%
HEP[2]	100.0	95.7	82.5	79.0	81.4	80.7	84.4	81.9	85.7[defgh]	7.7	9.0%
$\bar{x}$	*92.6*	*92.2*	*91.6*	*91.2*	*91.2*	*90.8*	*89.9*	*87.7*			
S	9.0	5.8	6.0	8.2	6.5	7.1	5.1	7.1			
CV	9.7%	6.3%	6.6%	9.0%	7.1%	7.8%	5.7%	8.1%			
C			0.0	-5.0	-5.2	-11.5	-24.2	-54.2			
B	0.0	-5.6	-13.9	-18.9	-19.1	-25.4	-38.1	-68.1			
A	1296.1	1290.5	1282.2	1277.2	1277.0	1270.7	1258.0	1228.0			
D	100.0%	99.6%	98.9%	98.5%	98.5%	98.0%	97.1%	94.7%			
E			0.0%	-0.4%	-0.4%	-0.9%	-1.9%	-4.2%			

[1]The lowest value is the most suitable; [2]the highest value is the most suitable. A = dye total score; B = point difference between dyes and CHLB; C = point difference between xanthophylls and LUT; D = percentage difference between dyes and CHLB; E = percentage difference between xanthophylls and LUT. Different letters in rows show statistical difference among property means ($p < 0.05$). [3]Standard deviation; [4]coefficient of variation.

There were 3 notable exceptions for the behavior described before. $f^{(2)}(r)^+$ and $f^{(2)}(r)^-$ conducted themselves in an erratic fashion, while ω^- increased instead of decreasing and HEP decreased instead of increasing.

ZEA-Hex experimental H-L (2.600 eV) was overestimated by 178% (4.632 eV) when CAM-B3LYP was employed. However, it is well known that long-range-corrected functionals overestimate H-L [40]. Regardless of this overestimation, these functionals are capable of helping with the calculations of other properties in the ground state. So, the accepted H-L values for our study are given by those calculated with B3P86 at the gas phase.

Generally in our work, the transition from a gas phase to a condensed phase leads to uniformity improvement of local reactivity indexes. f_k^+ showed a very uniform detection of the atom most prone to suffer a nucleophilic attack, since it was C(15′) in all BCRY and ZEA combinations. It was also the case for $f^{(2)}(r)^+$ in the first 4 combinations of BCRY, showing an excellent agreement with f_k^+. Index f_k^- indicated that the atom more prone to suffer an electrophilic attack was C(15) in the last 3 combinations of BCRY and ZEA, while $f^{(2)}(r)^-$ located that atom at C(15′) in all ZEA combinations. Eventually, f_k^0 exhibited that, like f_k^-, the atom most prone to suffer a radical attack was also C(15) in the last 4 combinations of BCRY and ZEA. Notably, condensed Fukui functions and condensed dual descriptor were in good agreement in a condensed phase.

The Marcus equation for electron transfer is a relation between the rate of outer-sphere electron transfer and the thermodynamics of this process. Essentially, the rate constant within the encounter complex (or the rate constant of intramolecular transfer) is given by the Eyring equation [41]:

$$k_{\mathrm{ET}} = \frac{\kappa_{\mathrm{ET}} kT}{h} \exp\left(\frac{\Delta G^{\ddagger}}{\mathrm{RT}}\right), \tag{3}$$

where k is the Boltzmann constant, h is the Planck constant, R is the gas constant, and κ_{ET} is the so-called electronic transmission factor ($\kappa_{\mathrm{ET}} \sim 1$ for adiabatic and $<<1$ for diabatic electron transfer). Through the pioneering seminal papers of Marcus Arthur Rudolph [42, 43], it is well established that the barrier height for outer-sphere electron transfer can be expressed as

$$\Delta G^{\ddagger} = \frac{\left(\lambda + \Delta_{\mathrm{ET}} G^0\right)^2}{4\lambda}, \tag{4}$$

where $\Delta_{\mathrm{ET}} G^0$ is the standard Gibbs energy change accompanying the electron-transfer reaction and λ is the total reorganization energy [44].

Table 4: Electronic properties of BCRY and ZEA in GP, Hex, Et_2O, Ace, EtOH, and MeOH (highest values of local reactivity indexes are given).

EP	BCRY GP	BCRY Hex	BCRY Et_2O	BCRY Ace	BCRY EtOH	BCRY MeOH	ZEA GP	ZEA Hex	ZEA Et_2O	ZEA Ace	ZEA EtOH	ZEA MeOH
H-L (eV)	4.633	4.629	4.625	4.621	4.620	4.620	4.635	4.632	4.628	4.624	4.624	4.623
I (eV)	5.775	5.279	4.971	4.782	4.774	4.764	5.812	5.304	4.987	4.792	4.783	4.773
A (eV)	1.550	2.077	2.456	2.733	2.747	2.762	1.591	2.105	2.474	2.744	2.757	2.773
χ (eV)	3.662	3.678	3.713	3.757	3.760	3.763	3.701	3.704	3.730	3.768	3.770	3.773
μ (eV)	-3.662	-3.678	-3.713	-3.757	-3.760	-3.763	-3.701	-3.704	-3.730	-3.768	-3.770	-3.773
η (eV)	2.112	1.601	1.257	1.025	1.014	1.001	2.110	1.600	1.256	1.024	1.013	1.000
S (eV)	0.473	0.625	0.795	0.976	0.987	0.999	0.473	0.625	0.796	0.977	0.987	1.000
ω (eV)	3.175	4.224	5.484	6.888	6.975	7.072	3.246	4.289	5.539	6.933	7.015	7.115
ω^- (eV)	3.921	3.895	3.914	3.954	3.956	3.959	3.961	3.922	3.931	3.964	3.967	3.969
ω^+ (eV)	1.196	1.608	1.976	2.283	2.300	2.318	1.226	1.631	1.992	2.295	2.310	2.328
$\Delta\omega^\pm$ (eV)	5.118	5.503	5.889	6.237	6.256	6.277	5.187	5.553	5.923	6.259	6.277	6.298
f_k^+	0.064	0.068	0.075	0.081	0.081	0.081	0.064	0.067	0.074	0.080	0.081	0.081
Atom	C(11)	C(15′)	C(15′)	C(15′)	C(15′)	C(15′)	C(11)	C(15′)	C(15′)	C(15′)	C(15′)	C(15′)
f_k^-	0.060	0.063	0.066	0.071	0.072	0.072	0.060	0.063	0.065	0.071	0.071	0.071
Atom	C(11′)	C(11′)	C(15)	C(15)	C(15)	C(15)	C(11′)	C(11′)	C(11′)	C(15)	C(15)	C(15)
f_k^0	0.062	0.064	0.070	0.076	0.076	0.076	0.062	0.064	0.069	0.075	0.076	0.076
Atom	C(11)	C(11′)	C(15)	C(15)	C(15)	C(15)	C(11)	C(11′)	C(15)	C(15)	C(15)	C(15)
$f^{(2)}(r)^+$	0.011	0.011	0.012	0.012	0.012	0.006	0.005	0.005	0.004	0.004	0.004	0.019
Atom	C(15′)	C(15′)	C(15′)	C(15′)	C(15′)	C(14′)	C(10′)	C(10′)	C(10′)	C(14′)	C(14′)	C(20′)
$f^{(2)}(r)^-$	-0.008	-0.007	-0.006	-0.006	-0.006	-0.012	-0.009	-0.009	-0.009	-0.010	-0.010	-0.010
Atom	C(10′)	C(10′)	C(10′)	C(14′)	C(14′)	C(15′)	C(15′)	C(15′)	C(15′)	C(15′)	C(15′)	C(15′)
s_k^+ (eV)	0.026	0.042	0.059	0.079	0.080	0.081	0.026	0.042	0.059	0.078	0.080	0.081
Atom	C(11)	C(15′)	C(15′)	C(15′)	C(15′)	C(15′)	C(11)	C(15′)	C(15′)	C(15′)	C(15′)	C(15′)
s_k^- (eV)	0.025	0.039	0.052	0.070	0.071	0.072	0.025	0.039	0.052	0.069	0.070	0.071
Atom	C(11′)	C(11′)	C(15)	C(15)	C(15)	C(15)	C(11′)	C(11′)	C(11′)	C(15)	C(15)	C(15)
s_k^0 (eV)	0.025	0.040	0.055	0.074	0.075	0.076	0.025	0.040	0.055	0.074	0.075	0.076
Atom	C(11)	C(11′)	C(15)	C(15)	C(15)	C(15)	C(11)	C(11′)	C(15)	C(15)	C(15)	C(15)
λ_e (eV)	0.655	0.619	0.592	0.573	0.572	0.570	0.663	0.624	0.595	0.575	0.575	0.574
EEP (eV)	2.205	2.696	3.048	3.306	3.319	3.332	2.254	2.729	3.070	3.319	3.332	3.347
λ_h (eV)	0.674	0.629	0.595	0.570	0.569	0.567	0.669	0.623	0.590	0.566	0.566	0.564
HEP (eV)	5.101	4.649	4.375	4.212	4.205	4.197	5.142	4.681	4.397	4.225	4.218	4.209

Hole reorganization energies for 6 pigments (containing ruthenium) that are used to sensitize solar cells were reported in the literature: 0.788 < 0.854 < 0.870 < 0.950 < 0.953 < 0.955 eV [45]. These values were obtained with an *ab initio* level of theory and acetonitrile as solvent. Our reorganization energies for electrons and holes were even smaller, which will be translated into an improved energy transfer, because most harvested energies by a donor will be used in electronic transitions and only a small part will be wasted in reorganization processes. Besides, more energy will be available to be transferred. All of it would increase the global efficiency of an artificial antenna. We strongly believe that the matrix shown in Table 4 (230 data, 23 properties multiplied by 10 combinations) will encourage other researchers to take advantage of it, in order to keep on expanding the knowledge frontier, in terms of the photosynthetic dye's performance as molecules isolated from their protein matrixes.

Considering that the dye's UV-Vis absorption spectra have a vibronic nature, a testing had to be performed in order to compare theoretical and experimental IR spectra. Figures 2–6 display experimental and theoretical IR spectra, and Figure 2 depicts BCRY experimental IR spectra; there are 3 main bands of minimal transmittance (%): the first band is located within 950-1050 cm^{-1}, the second one lies within 1350-1450 cm^{-1}, and the last one appears about 2900 cm^{-1}. The first band corresponds to the strong C-O

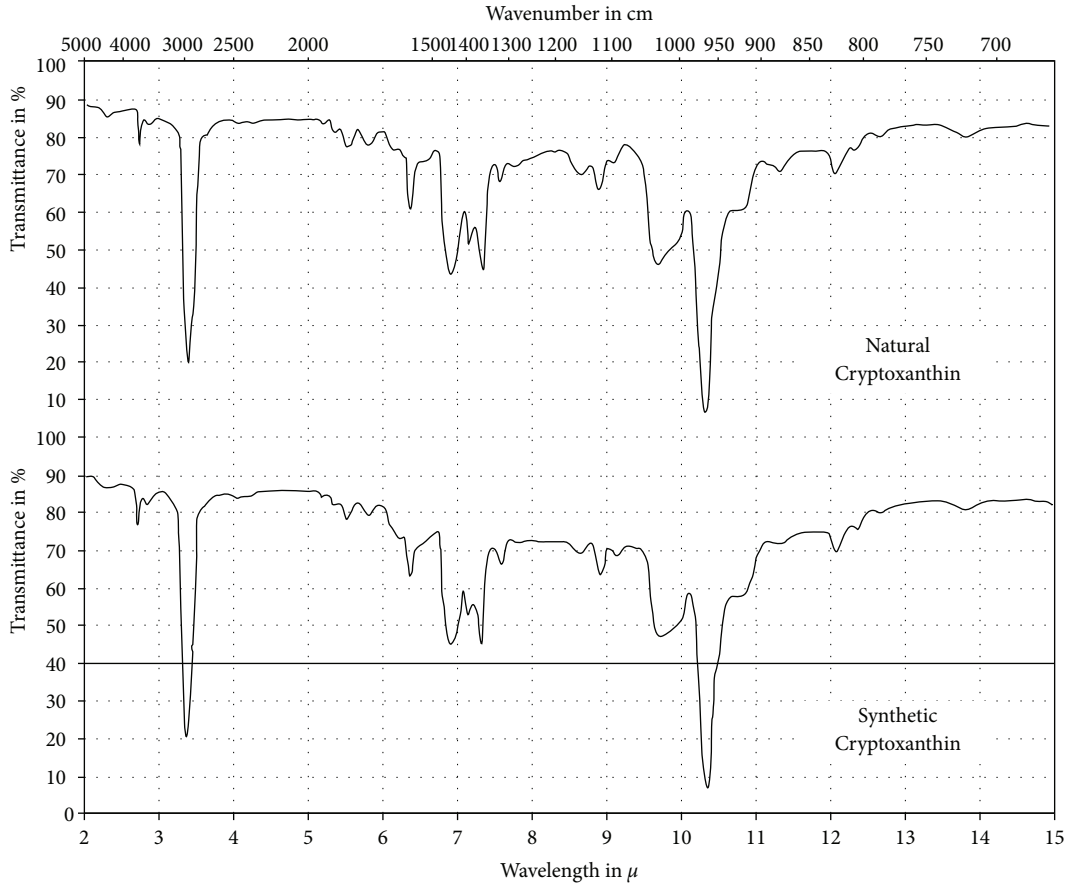

Figure 2: Experimental IR spectra of natural BCRY (at the upper part) and a synthetized BCRY (at the lower part). From 2 to 12 μ in chloroform and from 12 to 15 μ in carbon disulfide (solutions approximately at 1%, KBr cell plate spacing of 1 mm). Reproduced with the authorization of John Wiley and Sons Publisher [47].

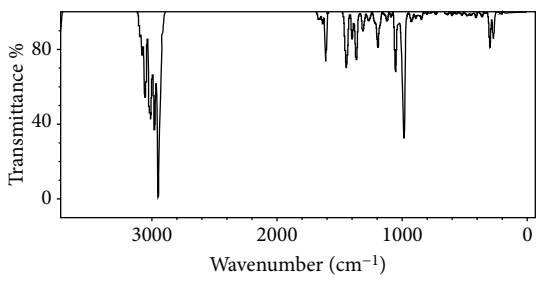

Figure 3: BCRY-MeOH theoretical IR spectrum.

stretching vibrational mode which is usually reported within 970-1250 cm^{-1}. The second band corresponds to the medium CH_2 and CH_3 deformation bending vibrational mode which is usually reported within 1350-1470 cm^{-1}, and the third band corresponds to the strong CH, CH_2, and CH_3 stretching vibrational mode whose energy falls within 2850-3000 cm^{-1} [46].

In Figure 3, the BCRY theoretical IR spectrum also presents the 3 bands of its counterpart, but differs from the former in intensity. In the experimental spectrum, the band height is at an approximate transmittance of 5, 45, and 15% whereas in our spectrum this height is about 30, 70, and 0%. So, our theoretical spectrum describes frequencies well, but the intensities of the first 2 bands are underestimated, while the last band intensity is slightly overestimated.

Figures 4 and 5 exhibit 2 experimental ZEA IR spectra; in Figure 4, there are 4 main bands of minimal transmittance (%): the first band is located at 909 cm^{-1}, the second one at 1464 cm^{-1}, the third one at 2852 cm^{-1}, and the last one at 3452 cm^{-1}. The first band corresponds to the strong =C-H bending vibrational mode which is usually reported within 880-995 cm^{-1}, the second band corresponds to the medium CH_2 and CH_3 deformation bending vibrational mode which is usually reported within 1350-1470 cm^{-1}, the third band corresponds to the strong CH, CH_2, and CH_3 stretching vibrational mode which is usually reported within 2850-3000 cm^{-1}, and the last band corresponds to the strong broad O-H (H-bonded) stretching vibrational mode which is usually reported within 3200-3550 cm^{-1} [46].

In Figure 5, there are 4 main bands of minimal transmittance (%): the first band (double-banded) is located about 1000 cm^{-1}, the second one (also double-banded) at ~1400 cm^{-1}, the third one around 2900 cm^{-1}, and the last one about 3400 cm^{-1}. The first band corresponds to the

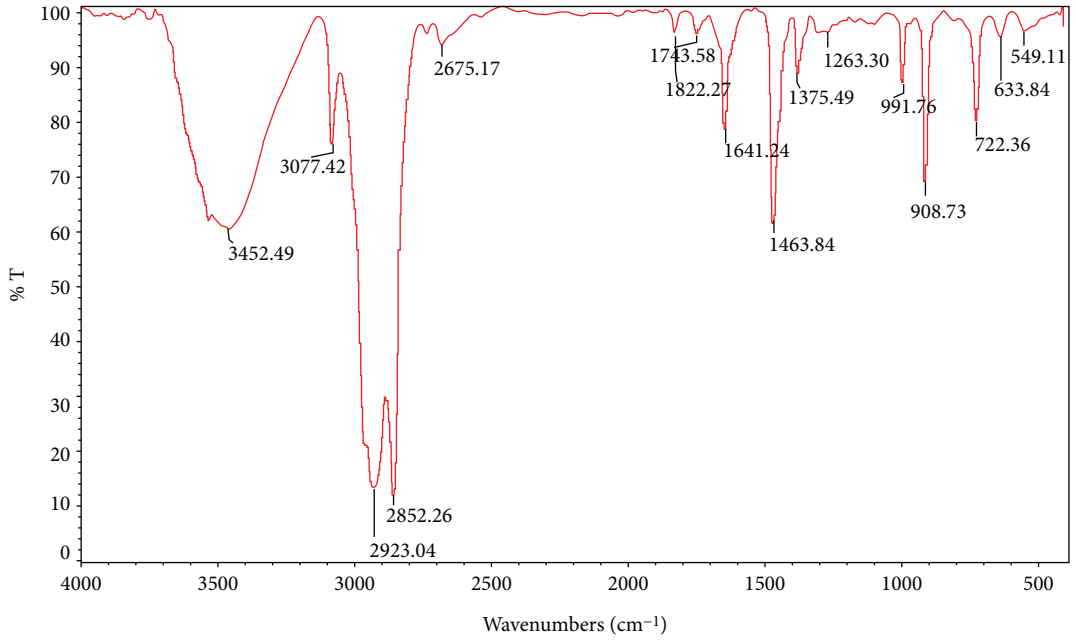

Figure 4: Experimental ZEA IR spectrum. Reproduced with the authorization of Universal Research Publications [48].

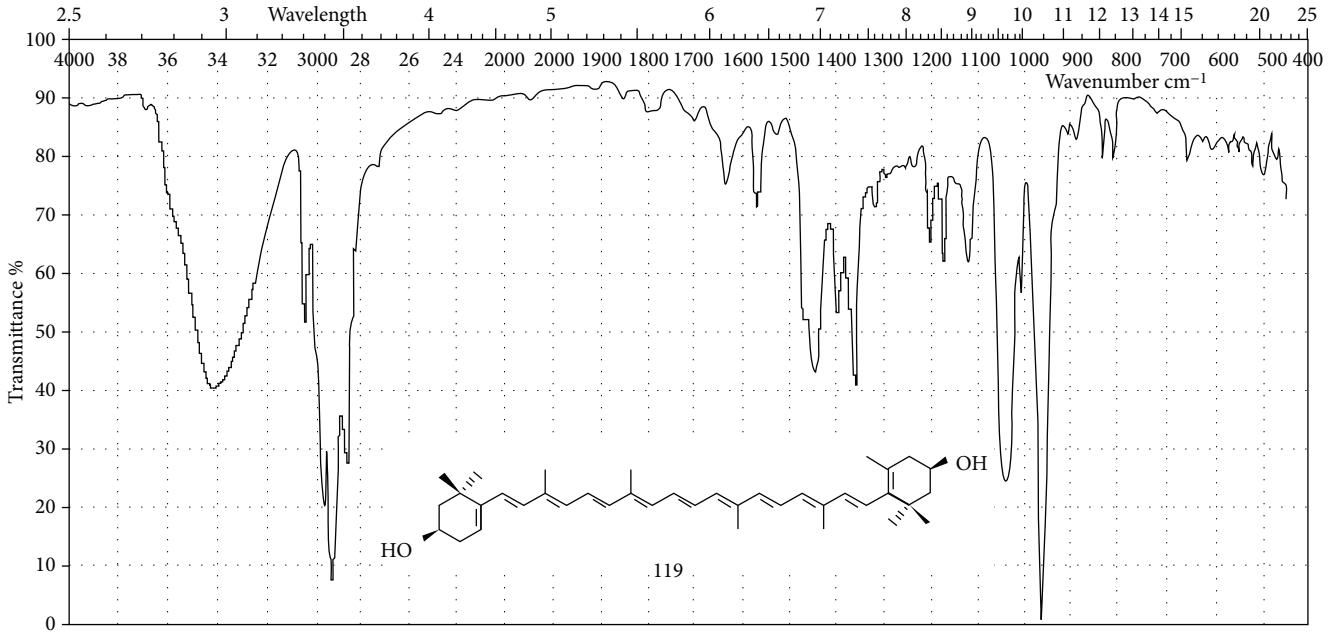

Figure 5: Experimental ZEA IR spectrum. Reproduced with the authorization of Birkhäuser Verlag AG Publisher [49].

strong C-O stretching vibrational mode which is usually reported within 970-1250 cm^{-1}. The second band corresponds to the medium CH_2 and CH_3 deformation bending vibrational mode which is usually reported within 1350-1470 cm^{-1}. The third band corresponds to the strong CH, CH_2, and CH_3 stretching vibrational mode which is usually reported within 2850-3000 cm^{-1}. The last band corresponds to the strong broad O-H (H-bonded) stretching vibrational mode which is usually reported within 3200-3550 cm^{-1} [46].

In Figure 6, the ZEA theoretical IR spectrum also shows the 4 bands of their counterparts, but differs from them in intensity. In the theoretical spectrum, the band height is at an approximate transmittance of 35, 75, 0, and 80% (despite the fact that this fourth band does not appear in Figure 6, its energy is 3857 cm^{-1}). The first experimental spectrum

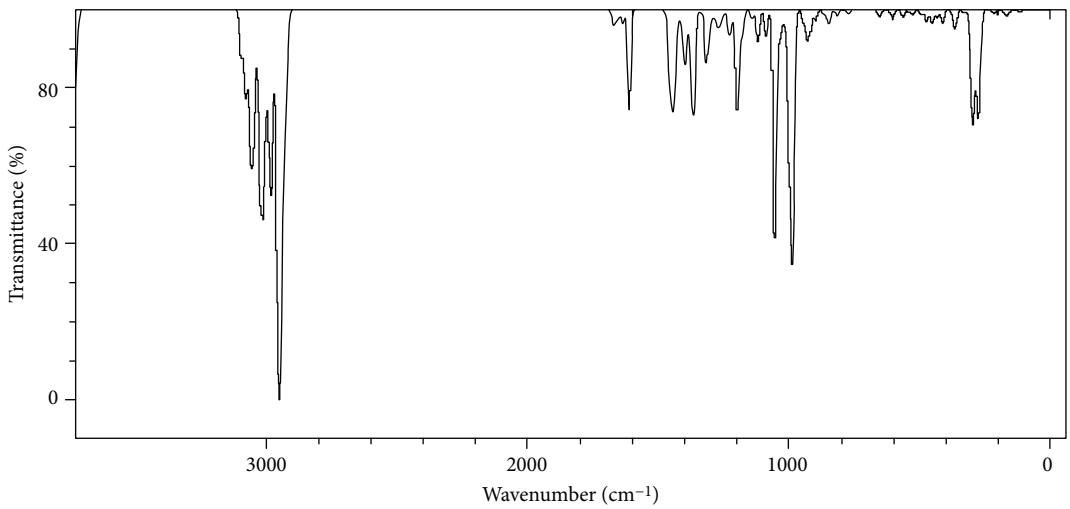

Figure 6: Theoretical ZEA-MeOH IR spectrum.

intensity is at a transmittance of 66, 62, 12, and 62%, while in the second experimental spectrum, intensity is at an approximate transmittance of 0, 40, 8, and 40%. Frequencies are generally described well; in the case of the fourth band, the PCM solvation model describes the solvent like a continuous surface charge instead of including explicit solvent molecules. The variable O-H (no hydrogen-bonded) normal vibrational mode lies within 3580-3650 cm^{-1} [46]. Our results indicate that the theoretical value is still about 207 nm further away. The main experimental bands' intensities are sometimes overestimated and other times underestimated. Finally, it is worth mentioning that the shapes of the theoretical spectrum's main bands resemble very well those found in the second experimental spectrum.

Focusing on Table 5, we can see that the main electronic transition of ZEA-Hex occurs at 2.532 eV (say, S_0-S_2/0-0 transition). The experimental reference is 2.600 eV, so that our calculation underestimated just 2.6% of the experimental value. This constitutes an indication that the electronic transition is essentially from HOMO to LUMO. The main electronic transition of ZEA-Ace is undertaken at 2.570 eV, and it can be inferred from its absorption spectrum [33]. Our study underestimated only 1.3% of this latter experimental value and also corresponds to an inherent electronic transition from HOMO to LUMO.

H-L electronic transitions are able to be compared with the lowest energy band of each experimental absorption spectrum (to say, 0-0 transition), since this band possesses the longest wavelength. From Table 5, we established the following order of combinations in accordance with the comparison against experiment, as long as experimental data were available in the literature: ZEA-Ace < ZEA-Hex-ZEA-EtOH < ZEA-MeOH-BCRY-Hex < BCRY-Ace < BCRY-EtOH. Moreover, the reasonable agreement between the theory and experiment also demonstrates that the vibrational contribution has been added successfully to the dye's vibronic spectra. ZEA was better described like an acceptor molecule by our methodology. As we will see in Figure 6 later on, BCRY-MeOH HOMO (-5.861 eV) has a higher energy than ZEA-MeOH HOMO (-5.873 eV) and ZEA-MeOH LUMO (-1.684 eV) has a lower energy than BCRY-MeOH LUMO (-1.674 eV). This behavior facilitates us to forecast that BCRY may be the donor molecule and ZEA the acceptor one in the future computational simulations.

As a finishing point of our discussion, Figure 7 exhibits the results from the analysis made with Chemissian software [50] in order to represent molecular orbitals of BCRY and ZEA using different solvents. Both molecules present the highest energy HOMO with the use of *n*-hexane as solvent, whereas methanol yields the lowest energy LUMO. *H-L* band gaps have similar values for both molecules as indicated in the figure. Despite *n*-hexane's performance at the time of augmenting the HOMO energy, methanol was our best option during the evaluation of dye properties' suitability (with a few exceptions).

4. Conclusions

This work reveals that the only higher plant's photosynthetic dyes that fit well into zeolite's nanochannels are BCRY and ZEA. Pigment's suitability to undergo both electronic transitions and electron transfer has the ordering at GP: CHLB > CHLA > LUT > NEO > ZEA > BCRY > VIO > 9NEO. Molecular properties' suitability improved as the dielectric constant of the solvent raised, and this effect allowed us to draw the conclusion that methanol was the best choice among the tested solvents to be employed in zeolite's future theoretical work. Furthermore, combinations' reorganization energies were low enough to forecast satisfactory energy transfer. BCRY's and ZEA's theoretical IR spectra described well the frequencies of the main bands (being O-H an exception), but they described poorly the intensity of these main bands. In any case, both theoretical IR spectra and experimental IR spectra matched good enough to expect a reasonable vibrational contribution to carotenoids' absorption spectra. The combinations'

Table 5: Three or 4 main electronic transitions of the selected pigments and comparisons versus experimental values (only electronic transitions with oscillator strengths (f) > 0.010 are shown).

Combination	Electronic transition	λ (nm)	Energy (eV)	f	Experimental values λ (nm)[1] [50]	$\Delta_{\lvert EXP\text{-}THE\rvert}$[2] (nm)
BCRY-Hex	1	490.0	2.530	4.767	(427), *452*, **478**	12
	2	265.8	4.664	0.467		
	3	287.1	4.319	0.155		
BCRY-Et_2O	1	488.8	2.537	4.785		
	2	265.3	4.673	0.455		
	3	287.2	4.317	0.154		
BCRY-Ace	1	489.2	2.534	4.785	(427), *450*, **475**	14
	2	265.3	4.674	0.444		
	3	287.6	4.311	0.161		
	4	242.5	5.113	0.109		
BCRY-EtOH	1	489.3	2.534	4.784	(428), *449*, **473**	16
	2	265.3	4.673	0.443		
	3	287.7	4.310	0.162		
	4	242.5	5.113	0.111		
BCRY-MeOH	1	487.4	2.544	4.803		
	2	264.8	4.682	0.441		
	3	287.4	4.314	0.153		
	4	242.5	5.114	0.111		
ZEA-Hex	1	489.7	2.532	4.774	(424), *450*, **478**	11
	2	265.8	4.665	0.474		
	3	286.2	4.333	0.145		
ZEA-EtOH	1	488.5	2.538	4.791		
	2	265.3	4.674	0.464		
	3	286.3	4.331	0.144		
ZEA-Ace	1	488.9	2.536	4.790	(428), *454*, **481**	8
	2	265.2	4.675	0.454		
	3	286.7	4.325	0.150		
	4	242.3	5.118	0.114		
ZEA-EtOH	1	489.0	2.535	4.789	(428), *450*, **478**	11
	2	265.2	4.675	0.453		
	3	286.7	4.324	0.151		
	4	242.3	5.118	0.114		
ZEA-MeOH	1	487.1	2.545	4.809	(429), *449*, **475**	12
	2	264.7	4.684	0.452		
	3	286.5	4.328	0.143		
	4	242.3	5.118	0.114		

[1]The values between parentheses correspond to the shoulder (the 0-2 transition), those in the italic font to the 0-1 transition, and those in the bold font to the 0-0 transition. All of them belong to the dye fine structure's absorption spectra. [2]Absolute difference between experimental and theoretical values (note that values have been rounded out similar to the experimental ones).

theoretical absorption spectra were in reasonable agreement with experimental S_0-S_2 electronic transitions, confirming the spectral vibrational contribution to these transitions. In light of our findings, we believe that there were two major implications. Firstly, data generated during the current study will allow both us and others to keep on researching different theoretical issues related to the field of artificial photosynthesis. Secondly, the theoretical methodology and results obtained throughout this computational effort constitute a suitable option in order to continue studying in depth both the geometrical and molecular properties of such natural dyes of extreme biochemical importance, particularly as molecules isolated from their higher plant lodging.

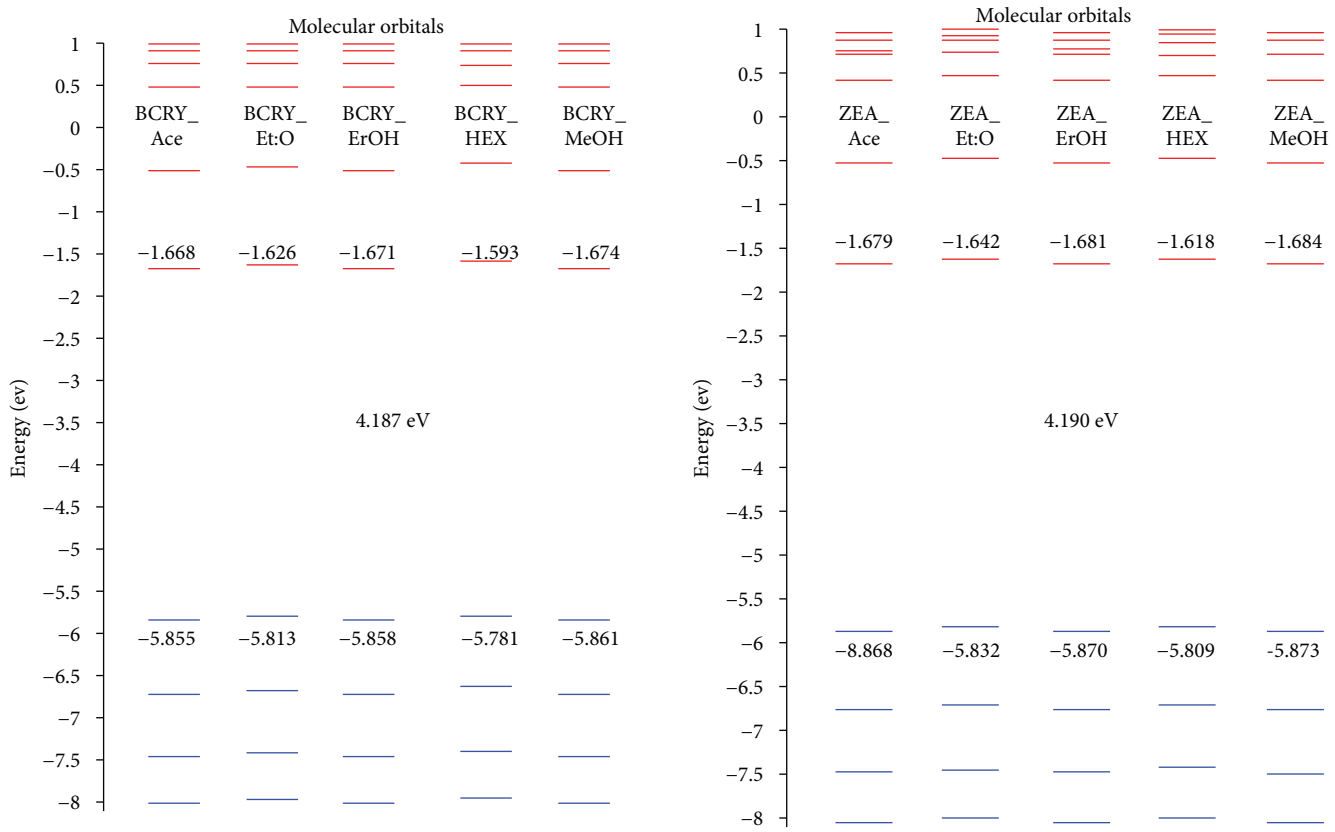

Figure 7: Molecular orbital energies (eV) of combinations in the ground state.

Data Availability

We are sharing data within this site: https://drive.google.com/open?id=10MtIOn7nmkMwAwX_NdzWZRhGMnSQts-O. Our research group is willing to share data if needed; please contact Dr. Diana Barraza at diana.barraza@ujed.mx. We are sharing what we considered the more representative data in the site and are willing to share further data if requested. Please contact Dr. Diana Barraza if there is any comment regarding the data shared.

Conflicts of Interest

The authors state that this research was completed without any conflicts of interest because of the received funding.

Acknowledgments

JFMB would like to thank CONACYT (Mexican Science and Technology National Council) for a doctorate scholarship. The authors would like to thank CONACYT SEP-CB (Basic Science-Public Education Ministry) for funding this project with 158307 grant. Thanks are due to the Scientific Computational Laboratory at FCQ-UJED for computational resources. Thanks are due to Academic Group UJED-CA-129 for valuable discussions.

Supplementary Materials

Additional data including Cartesian coordinates for each molecular structure, concept, and equation for energy calculations. Table 1: CHLA Cartesian coordinates. Table 2: CHLB Cartesian coordinates. Table 3: BCRY Cartesian coordinates. Table 4: ZEA Cartesian coordinates. Table 5: LUT Cartesian coordinates. Table 6: VIO Cartesian coordinates. Table 7: 9NEO Cartesian coordinates. Table 8: NEO Cartesian coordinates. *(Supplementary Materials)*

References

[1] M. Z. Jacobson, *Air Pollution and Global Warming: History, Science, and Solutions*, Cambridge University Press, New York, NY, USA, 2nd edition, 2012.

[2] D. Gust, T. A. Moore, and A. L. Moore, "Solar fuels via artificial photosynthesis," *Accounts of Chemical Research*, vol. 42, no. 12, pp. 1890–1898, 2009.

[3] L. Taiz and E. Zeiger, *Plant Physiology*, Sinauer Associates Inc, Sunderland, MA, USA, 2006.

[4] R. E. Blankenship, *Molecular Mechanisms of Photosynthesis*, WILEY Blackwell, Chichester, 2014.

[5] T. Polivka, J. L. Herek, D. Zigmantas, H.-E. Akerlund, and V. Sundstrom, "Direct observation of the (forbidden) S_1 state in carotenoids," *Proceedings of the National Academy of Sciences*, vol. 96, no. 9, pp. 4914–4917, 1999.

[6] H. E. Khoo, K. N. Prasad, K. W. Kong, Y. Jiang, and A. Ismail, "Carotenoids and their isomers: color pigments in fruits and vegetables," *Molecules*, vol. 16, no. 2, pp. 1710–1738, 2011.

[7] Z. Liu, H. Yan, K. Wang et al., "Crystal structure of spinach major light-harvesting complex at 2.72 Å resolution," *Nature*, vol. 428, no. 6980, pp. 287–292, 2004.

[8] C. C. Gradinaru, I. H. M. van Stokkum, A. A. Pascal, R. van Grondelle, and H. van Amerongen, "Identifying the pathways of energy transfer between carotenoids and chlorophylls in LHCII and CP29. A multicolor, femtosecond pump−probe study," *The Journal of Physical Chemistry. B*, vol. 104, no. 39, pp. 9330–9342, 2000.

[9] J. Martiskainen, R. Kananavičius, J. Linnanto et al., "Excitation energy transfer in the LHC-II trimer: from carotenoids to chlorophylls in space and time," *Photosynthesis Research*, vol. 107, no. 2, pp. 195–207, 2011.

[10] A. F. Collings and C. Critchley, *Artificial Photosynthesis: From Basic Biology to Industrial Application*, Wiley-VCH, Weinheim, 2005.

[11] G. Calzaferri, "Artificial photosynthesis," *Topics in Catalysis*, vol. 53, no. 3-4, pp. 130–140, 2010.

[12] T. Ruiz-Anchondo, N. Flores-Holguín, and D. Glossman-Mitnik, "Natural carotenoids as nanomaterial precursors for molecular photovoltaics: a computational DFT study," *Molecules*, vol. 15, no. 7, pp. 4490–4510, 2010.

[13] F. Torres-Rivas, M. A. Flores-Hidalgo, D. Glossman-Mitnik, and D. Barraza-Jimenez, "Geometric description and electronic properties of the principal photosynthetic pigments of higher plants: a DFT study," *Journal of Molecular Modeling*, vol. 21, no. 10, p. 256, 2015.

[14] M. J. Frisch, G. W. Trucks, H. B. Schlegel et al., *Gaussian 09, D.01 Revision*, Gaussian Inc., Wallingford, CT, USA, 2009.

[15] P. Hohenberg and W. Kohn, "Inhomogeneous electron gas," *Physical Review B*, vol. 136, no. 3B, pp. B864–B871, 1964.

[16] R. Bauernschmitt and R. Ahlrichs, "Treatment of electronic excitations within the adiabatic approximation of time dependent density functional theory," *Chemical Physics Letters*, vol. 256, no. 4-5, pp. 454–464, 1996.

[17] D. Glossman-Mitnik, "Computational chemistry of natural products: a comparison of the chemical reactivity of isonaringin calculated with the M06 family of density functionals," *Journal of Molecular Modeling*, vol. 20, no. 7, p. 2316, 2014.

[18] M. Wormit, P. H. P. Harbach, J. M. Mewes, S. Amarie, J. Wachtveitl, and A. Dreuw, "Excitation energy transfer and carotenoid radical cation formation in light harvesting complexes - a theoretical perspective," *Biochimica et Biophysica Acta (BBA) - Bioenergetics*, vol. 1787, no. 6, pp. 738–746, 2009.

[19] K. R. Cousins, "Computer review of ChemDraw ultra 12.0.," *Journal of the American Chemical Society*, vol. 133, no. 21, pp. 8388–8388, 2011.

[20] S. A. Zygmunt, R. M. Mueller, L. A. Curtiss, and L. E. Iton, "An assessment of density functional methods for studying molecular adsorption in cluster models of zeolites," *Journal of Molecular Structure: THEOCHEM*, vol. 430, pp. 9–16, 1998.

[21] J. P. Perdew, "Density-functional approximation for the correlation energy of the inhomogeneous electron gas," *Physical Review B*, vol. 33, no. 12, pp. 8822–8824, 1986.

[22] A. D. Becke, "Density-functional thermochemistry. III. The role of exact exchange," *The Journal of Chemical Physics*, vol. 98, no. 7, pp. 5648–5652, 1993.

[23] R. Ditchfield, W. J. Hehre, and J. A. Pople, "Self-consistent molecular-orbital methods. IX. An extended gaussian-type basis for molecular-orbital studies of organic molecules," *The Journal of Chemical Physics*, vol. 54, no. 2, pp. 724–728, 1971.

[24] P. Geerlings, F. De Proft, and W. Langenaeker, "Conceptual density functional theory," *Chemical Reviews*, vol. 103, no. 5, pp. 1793–1874, 2003.

[25] J. Hintze, *NCSS, PASS and GESS, NCSS Statistical Software*, Kaysville, UT, USA, 2006, http://www.NCSS.com.

[26] T. Yanai, D. P. Tew, and N. C. Handy, "A new hybrid exchange-correlation functional using the Coulomb-attenuating method (CAM-B3LYP)," *Chemical Physics Letters*, vol. 393, no. 1-3, pp. 51–57, 2004.

[27] A. D. McLean and G. S. Chandler, "Contracted Gaussian basis sets for molecular calculations. I. Second row atoms, Z=11–18," *The Journal of Chemical Physics*, vol. 72, no. 10, pp. 5639–5648, 1980.

[28] C. D. P. Duffy, L. Valkunas, and A. V. Ruban, "Quantum mechanical calculations of xanthophyll-chlorophyll electronic coupling in the light-harvesting antenna of photosystem II of higher plants," *The Journal of Physical Chemistry. B*, vol. 117, no. 25, pp. 7605–7614, 2013.

[29] J. P. Götze and W. Thiel, "TD-DFT and DFT/MRCI study of electronic excitations in violaxanthin and zeaxanthin," *Chemical Physics*, vol. 415, pp. 247–255, 2013.

[30] B. Mennucci, "Polarizable continuum model," *Wiley Interdisciplinary Reviews: Computational Molecular Science*, vol. 2, no. 3, 2012.

[31] D. C. Giancoli, *Physics for Scientists and Engineers with Modern Physics*, Pearson Education INC. Prentice Hall INC, New Jersey, 2008.

[32] C. A. Gueymard, "The sun's total and spectral irradiance for solar energy applications and solar radiation models," *Solar Energy*, vol. 76, no. 4, pp. 423–453, 2004.

[33] H. A. Frank, J. A. Bautista, J. S. Josue, and A. J. Young, "Mechanism of nonphotochemical quenching in green plants: energies of the lowest excited singlet states of violaxanthin and zeaxanthin," *Biochemistry*, vol. 39, no. 11, pp. 2831–2837, 2000.

[34] G. K. Ramachandran, J. K. Tomfohr, J. Li et al., "Electron transport properties of a carotene molecule in a metal–(single molecule)–metal junction," *The Journal of Physical Chemistry. B*, vol. 107, no. 25, pp. 6162–6169, 2003.

[35] C. Houssier and K. Sauer, "Circular dichroism and magnetic circular dichroism of the chlorophyll and protochlorophyll pigments," *Journal of the American Chemical Society*, vol. 92, no. 4, pp. 779–791, 1970.

[36] R. S. Mulliken, "A new electroaffinity scale; together with data on valence states and on valence ionization potentials and electron affinities," *The Journal of Chemical Physics*, vol. 2, no. 11, pp. 782–793, 1934.

[37] R. G. Parr and R. G. Pearson, "Absolute hardness: companion parameter to absolute electronegativity," *Journal of the American Chemical Society*, vol. 105, no. 26, pp. 7512–7516, 1983.

[38] R. G. Parr, L. . Szentpály, and S. Liu, "Electrophilicity index," *Journal of the American Chemical Society*, vol. 121, no. 9, pp. 1922–1924, 1999.

[39] J. L. Gázquez, A. Cedillo, and A. Vela, "Electrodonating and electroaccepting powers," *The Journal of Physical Chemistry. A*, vol. 111, no. 10, pp. 1966–1970, 2007.

[40] H. Sekino, Y. Maeda, M. Kamiya, and K. Hirao, "Polarizability and second hyperpolarizability evaluation of long molecules by the density functional theory with long-range correction," *The Journal of Chemical Physics*, vol. 126, no. 1, article 014107, 2007.

[41] H. Eyring, "The activated complex and the absolute rate of chemical reactions," *Chemical Reviews*, vol. 17, no. 1, pp. 65–77, 1935.

[42] R. A. Marcus, "On the theory of oxidation-reduction reactions involving electron transfer. I," *The Journal of Chemical Physics*, vol. 24, no. 5, pp. 966–978, 1956.

[43] R. A. Marcus, "Chemical and electrochemical electron-transfer theory," *Annual Review of Physical Chemistry*, vol. 15, no. 1, pp. 155–196, 1964.

[44] M. Nic, J. Jirat, B. Kosata, A. D. McNaught, A. Wilkinson, and A. Jenkins, *Compendium of Chemical Terminology, IUPAC, Gold Book*, Blackwell Scientific Publications, Oxford, 2nd edition, 1997.

[45] V. Vaissier, P. Barnes, J. Kirkpatrick, and J. Nelson, "Influence of polar medium on the reorganization energy of charge transfer between dyes in a dye sensitized film," *Physical Chemistry Chemical Physics*, vol. 15, no. 13, pp. 4804–4814, 2013.

[46] G. Socrates, *Infrared and Raman Characteristic Group Frequencies. Tables and Charts*, John Wiley and Sons, Ltd., Chichester, 3rd Edition edition, 2001.

[47] O. Isler, H. Lindlar, M. Montavon, R. Rüegg, G. Saucy, and P. Zeller, "Synthesen in der carotinoid-reihe. 8. Mitteilung. Total synthese von kryptoxanthin und eine weitere synthese von zeaxanthin," *Helvetica Chimica Acta*, vol. 40, no. 2, pp. 456–467, 1957.

[48] P. Arunkumar and A. Yogamoorthi, "Isolation, application and biochemical characterization of colour component from *Tecoma stans*: a new cost effective and eco-friendly source of natural dye," *International Journal of Natural Products Research*, vol. 4, no. 1, pp. 9–13, 2014.

[49] K. Bernhard and M. Grosjean, *Carotenoids Vol. 1B: Spectroscopy Chapter 4: IR Spectroscopy*, G. Britton, S. Liaaen-Jensen, and H. Pfander, Eds., Birkhäuser Verlag AG, Springer Basel AG, Basel, Switzerland, 1995.

[50] S. Roy, C. A. Llewellyn, E. S. Egeland, and G. Johnsen, *Phytoplankton Pigments: Characterization, Chemotaxonomy and Applications in Oceanography*, Cambridge University Press, New York, NY, USA, 2011.